Chinese Journal of Chemical Engineering 56 (2023) 255–265

Contents lists available at ScienceDirect

Chinese Journal of Chemical Engineering

journal homepage: www.elsevier.com/locate/CJChE

Full Length Article

Microfluidic field strategy for enhancement and scale up of liquid–liquid homogeneous chemical processes by optimization of 3D spiral baffle structure

Shuangfei Zhao [1], Yingying Nie [1], Wenyan Zhang [1], Runze Hu [1], Lianzhu Sheng [1], Wei He [1], Ning Zhu [1,2], Yuguang Li [3], Dong Ji [3], Kai Guo [1,2,*]

[1] College of Biotechnology and Pharmaceutical Engineering, Nanjing Tech University, Nanjing 211816, China
[2] State Key Laboratory of Materials-Oriented Chemical Engineering, Nanjing Tech University, Nanjing 211816, China
[3] Institute of Nanjing Advanced Biomaterials & Processing Equipment, Nanjing 211299, China

ARTICLE INFO

Article history:
Received 15 March 2022
Received in revised form 3 July 2022
Accepted 15 July 2022
Available online 22 July 2022

Keywords:
Mixing efficiency
Chemical process intensification
Scale up
Reactor
Computational fluid dynamics (CFD)
Numerical simulation

ABSTRACT

Due to the scale effect, the uniform distribution of reagents in continuous flow reactor becomes bad when the channel is enlarged to tens of millimeters. Microfluidic field strategy was proposed to produce high mixing efficiency in large-scale channel. A 3D spiral baffle structure (3SBS) was designed and optimized to form microfluidic field disturbed by continuous secondary flow in millimeter scale Y-shaped tube mixer (YSTM). Enhancement effect of the 3SBS in liquid–liquid homogeneous chemical processes was verified and evaluated through the combination of simulation and experiment. Compared with 1 mm YSTM, 10 mm YSTM with 3SBS increased the treatment capacity by 100 times, shortened the basic complete mixing time by 0.85 times, which proves the potential of microfluidic field strategy in enhancement and scale-up of liquid–liquid homogeneous chemical process.

1. Introduction

Chemical industry, plays a key role in promoting the progress of human society [1,2]. However, chemical process in batch reactor limits it from solving problems both classical and new, such as poor selectivity, complex stepwise operation, wastes of resources, poor reproducibility, and safety concerns. Continuous flow reactors with scale no more than 1 mm have great potential in green and smart chemical process [3,4]. Due to its precisely controlled reaction parameter, rapid mixing and heat/mass transfer, and minimal reagent consumption, microreactors have been widely used for organic synthesis [5–7], microscale and nanoscale material preparation [8–11], pollutant extraction [12,13] and biomedical applications [14,15]. Recently, the demand for continuous flow reactors for industrial production is increasing. However, due to competition mechanism between quality and yield, it is difficult to realize industrial production with small size reactor.

At present, there are several ways to improve the output of continuous flow microreactor [16,17]. The first way is the increase of the number of original micro reaction system directly through external parallel connection, by which each reaction unit is capable of working alone and achieving high quality products [18,19]. However, the cost of this method is relatively high. The second way is the realization of multi-channel high-throughput preparation by internal shunt without changing the number of supporting hardware. This method has higher requirements for a uniform flow distribution of reagents [20–22]. The third way is to enlarge the pipe diameter or increase the fluid flow. In this way, the high mixing efficiency of the reaction liquid needs to be realized in a larger pipe diameter or higher flow rate [23–25]. Considering the equipment cost and shunt technical difficulties, continuous flow reactor with large diameter and high flow rate has potential in scale-up of chemical process. Therefore, the chemical process intensification technology based on larger diameter and high flow rate is in urgent need of research.

Mixing efficiency of reaction reagents plays a significant role in the liquid–liquid homogeneous chemical process [26–28]. Mixing efficiency can be enhanced in small size reactors by optimizing the channel structure, despite the absence of turbulence [29,30]. The molecular diffusion and chaotic advection of reagents can be increased by an enhancement in the contact surface between the fluids and a reduction in the mixing distance [31]. Until now, many special structures, such as lamination based, obstacle based,

* Corresponding author.
E-mail address: guok@njtech.edu.cn (K. Guo).

https://doi.org/10.1016/j.cjche.2022.07.016
1004-9541/

curved-channel, convergence-divergence based, unsymmetrical and droplet based, have been proposed for mixing enhancement of microreactors by numerical and experimental investigations [32–37]. However, detailed information concerning secondary flow disturbance mechanism with continuous change of direction in large scale reactor is still lacking.

In this study, the scale effect of Y-shaped tube mixer (YSTM) will be studied to reveal the competition mechanism between distribution uniformity and treatment capacity. The microfluidic field strategy is proposed and expected to achieve scale-up on the premise of ensuring high mixing efficiency in homogeneous chemical process. The microfluidic field strategy will be adopted to enhance and enlarge the continuous flow chemical process in a millimeter scale YSTM. The secondary flow disturbance mechanism with continuous change of direction in large scale reactor will be studied, and a 3D spiral baffle structure (3SBS) will be designed and optimized. The enhancement effects of the microfluidic field strategy will be verified by comparing with the diameter of 1 mm and studied by combination of computational fluid dynamics (CFD) numerical simulation and validation experiment.

2. Methodology

2.1. Design of microfluidic field geometry model

Due to the centrifugal force, it will produce a pair of secondary flow vortices with opposite rotation direction along the uneven wall, which is called Goertler vortex [38]. In this work, 3SBS is designed to induce the secondary flow of the Goertler vortex with continuously changing direction, which has great potential to promote fluid mixing. The basic channel geometry in the present work is a kind of YSTM, of which the internal fluid region is shown in Fig. 1(a). The diameter and length of the mixer are indicated by D_Y and L, respectively.

In order to enhance the mixing efficiency in 10 mm YSTM, a microfluidic field strategy is proposed in this study. The internal fluid region and the geometry of 10 mm YSTM with 3SBS are shown in Fig. 1(b) and (c). The 3SBS has four spiral baffle units, and the spiral baffle unit is formed by rotating and stretching the spiral plane on the radial section of the tube. The rotation angle between the initial plane (IP) and the final plane (FP) is indicated by θ_1. The thickness and spiral baffle unit length of 3SBS are indicated by a and L_s. The latter unit rotates θ_2 along the radial direction of the tube on the basis of the former unit. The detailed geometry of 3SBS is shown in Fig. 1(d).

2.2. Governing equations

The flow laws of viscous fluid in tubes are governed by the following Navier–Stokes (N–S) equations including momentum balance equation, continuity equation and mass conservation equation:

$$\rho(\boldsymbol{u}\cdot\nabla)\boldsymbol{u}+\nabla p-\eta\nabla\cdot\nabla\boldsymbol{u}=0 \tag{1}$$

$$\nabla\cdot\boldsymbol{u}=0 \tag{2}$$

$$\nabla\cdot(D\nabla c)=\boldsymbol{u}\cdot\nabla c \tag{3}$$

where $\boldsymbol{u}$ is the velocity vector, ρ is the fluid density, η is the dynamic viscosity, and p is the pressure, c is the concentration, D is diffusion coefficient.

2.3. Computational fluid dynamics simulation settings

The mixing performances were studied by numerical simulation using ANSYS/FLUENT. The laminar flow model was used for the simulations. The pressure-based solver and steady state calculation were adopted. The two inlets were set as velocity-inlet, and the outlet was set as pressure-outlet, the rest faces were defined as wall. The species transport model was adopted for the mixing process. Liquid water with density of 1000 $kg\cdot m^{-3}$ and viscosity of 0.001 $kg\cdot m^{-1}\cdot s^{-1}$ was selected as the representative fluid. The two inlets were injected with liquid water, and the mass fractions were set to 0 and 1, respectively. The mass diffusivity coefficient was set to 1.0×10^{-9} $m^2\cdot s^{-1}$. In the simulation, finite volume method was adopt as the interpolation scheme. The convergence criteria for all equations were 10^{-3}. After all the parameters were set, initialize the calculations and start iteration, and when the iterations converge, analyze the results. Intel Xeon Gold 5118 @ 2.30 GHz with 12 cores and 48 GB RAM memory were used in the numerical simulations.

The mixing performance of the fluids can be characterized by the standard deviation of fluid concentration [39]. To establish the quantitative standard of mixing uniformity suitable for any flow velocity ratio, the standard deviation formula was modified and normalized as follow [40]:

$$M=1-\sqrt{\frac{1}{N}\sum_{1}^{N}\left(\frac{c_i-c_{\mathrm{mix}}}{c_{\mathrm{unmix}}-c_{\mathrm{mix}}}\right)^2} \tag{4}$$

where M is the mixing efficiency index, N is the total number of sampling points, c_i is the mass fraction of the selected points, c_{mix} is the expected mass fraction of fluids after mixing, and c_{unmix} is the initial mass fraction of fluids, respectively.

In multi-step liquid–liquid homogeneous chemical reactions, the competitive behavior of chemical reactions and the yield of chemical products are not only affected by the mixing efficiency, but also by the time required to achieve high mixing efficiency. The mixing time (t) of fluid in the channel can be calculated by the following equation:

$$t=\frac{L}{v_{\mathrm{t}}} \tag{5}$$

where v_{t} is the total flow velocity, $m\cdot s^{-1}$, L is the total length of mixer.

In order to further quantify the enhancement effect of 3SBS, time and length required for efficient mixing of fluids are utilized and calculated. When the fluid mixing efficiency reaches 0.9, it is defined as basically complete mixing state. The time and length of the fluid to reach the basic complete mixing state are $t_{0.9}$ and $L_{0.9}$ respectively.

Furthermore, the treatment capacity (Q_{t}) refers to the total volume of fluid flowing into the mixer from two inlets per unit time. And it can be calculated by the following equation:

$$Q_{\mathrm{t}}=Av_{\mathrm{t}}=\frac{\pi D_{\mathrm{Y}}^2}{4}v_{\mathrm{t}} \tag{6}$$

where A is the radial sectional area of the inlet. The increase of D_Y and v_{t} is beneficial to the increase of Q_{t}.

2.4. Mesh independence testing

In this test, the mesh is divided by Mesh module in Workbench. In order to determine the appropriate mesh size (S_{m}) for simulation of mixing efficiency, S_{m} was gradually reduced. The total flow velocity was fixed at 0.01 $m\cdot s^{-1}$ and flow velocity ratio was fixed at 1.The total lengths of mixing zone of YSTM with and without 3SBS were fixed at 110 mm. The maximum aspect ratio, minimum orthogonal quality, and maximum skewness of the meshes are 55.1, 0.063 and 0.9, respectively. The detailed meshes of 10 mm YSTM with and without 3SBS are shown in Fig. 2(a) and (b).

When S_{m} is gradually reduced from 0.20 to 0.05, the number of mesh gradually increases. For the 1 mm YSTM, the mixing effi-

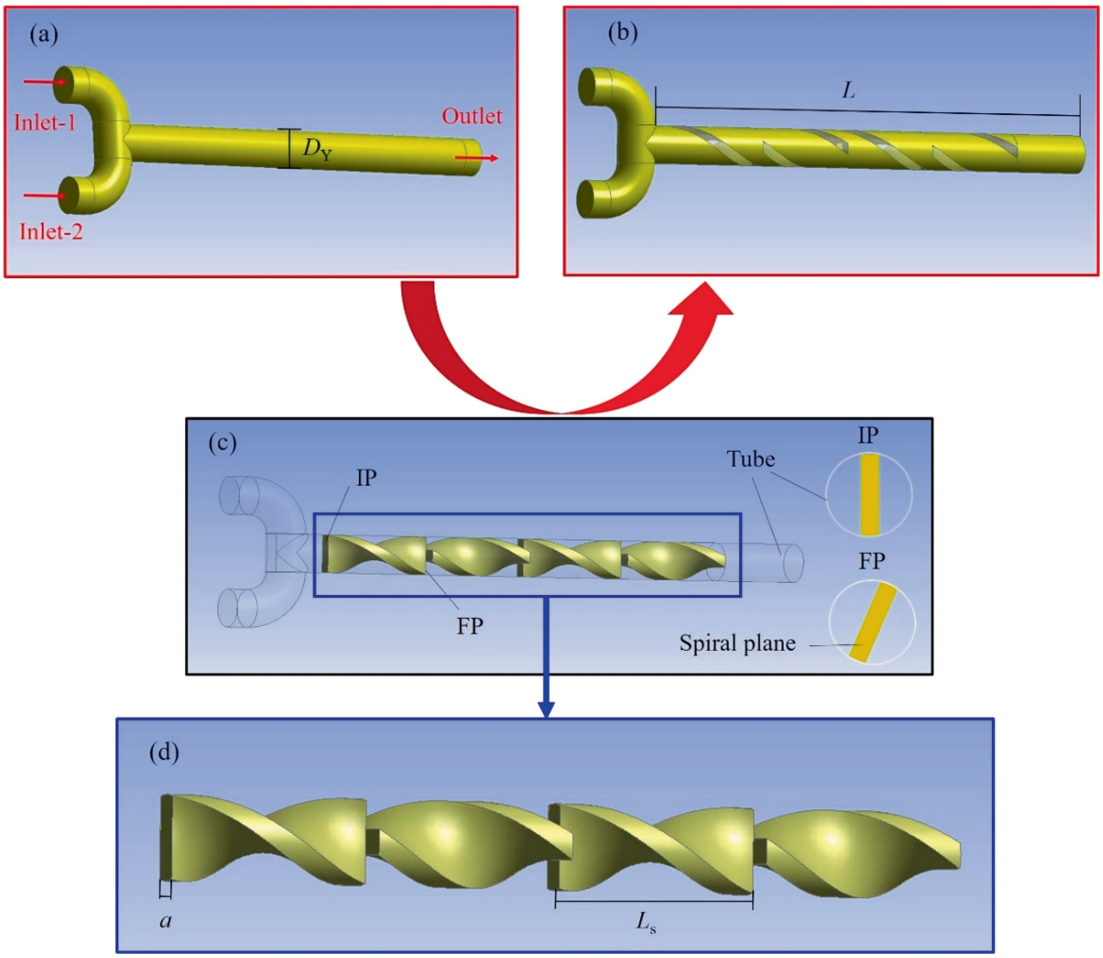

Fig. 1. (a) Internal fluid region of YSTM without 3SBS; (b) internal fluid region of YSTM with 3SBS; (c) channel geometry of YSTM with 3SBS; (d) geometry of 3SBS.

ciency of the radial section at 5 mm length is selected for the mesh independence study. For the other mixers, the length is 30 mm. After adjusting the elements of mesh, the results of mixing efficiency index are shown in Fig. 2(c). With the increase of the elements of mesh, the mixing efficiency index and variation rate decrease gradually. Considering the independence of the mesh and the amount of computation, the optimal mesh elements of 1, 3, 5, 8, 10 mm YSTM without 3SBS and 10 mm YSTM with 3SBS are determined as 1.12×10^6, 1.07×10^6, 7.02×10^5, 4.99×10^5, 8.40×10^5 and 8.81×10^5, respectively.

2.5. Validation experiments

2.5.1. Experimental setup

As shown in Fig. 3, the experimental setup in verification experiments consists of two pumps (TYD01-01-CE, Baoding Leifu Fluid Technology Co., ltd., China), the mixer and its connecting pipeline. Due to its complex baffle structure, the mixer is fabricated by 3D printing technology (Lite 600, Shanghai Union Technology Co., ltd., China). The mixer and pump are connected by PTFE pipe with outer diameter of 3.2 mm and inner diameter of 1.6 mm. The mixer and PTFE pipe are connected by M6 thread. The experiment was carried out at 25 ℃.

2.5.2. Homogeneous experiment

The Villermaux–Dushman parallel competing reaction was used to evaluate the homogeneous case. The chemical reaction equations are as follows:

$$H^+ + H_2BO_3^- \rightarrow H_3BO_3 \quad (a)$$

$$5I^- + 6H^+ + IO_3^- \rightarrow 3I_2 + 3H_2O \quad (b)$$

$$I^- + I_2 \rightleftharpoons I_3^- \quad (c)$$

The Villermaux–Dushman procedure implies the addition of a small quantity of H^+ to a mixture of iodate, iodide and borate ions. The amount of H^+ added is in stoichiometric deficiency to make sure reactions (a) and (b) will go in competition. In perfect mixing conditions, the H^+ is immediately dispersed and consumed by the instantaneous reaction (reaction (a)). When nonideal mixing conditions occur, the mixing time is in the same range or higher than the characteristic reaction time of reaction (b). A local overconcentration of the H^+ will exist and the H^+ will react with iodide and iodate to yield iodine. Due to the excess of iodide, all iodine is transformed into triiodide according to reaction (c). Therefore, the segregation index (X_s, as calculated by Eq. (7)) can be defined as a quantitative indicator for mixing performance [35,41,42].

$$X_s = \frac{Y}{Y_{ST}} = \frac{\left(VC_{I_2} + C_{I_3^-}\right)}{n_{H^+,0}} \left(\frac{6C_{IO_3^-,0} + C_{H_2BO_3^-,0}}{3C_{IO_3^-,0}}\right) \quad (7)$$

where Y represents the ratio of the amount of H^+ consumed by reaction (b) over the total amount of H^+ added to the solutions; Y_{ST} represents the value of Y in the case of total segregation; V represents the total volume of the solution; n represents the mole number; C represents the mole concentration of the subscript species. If X_s

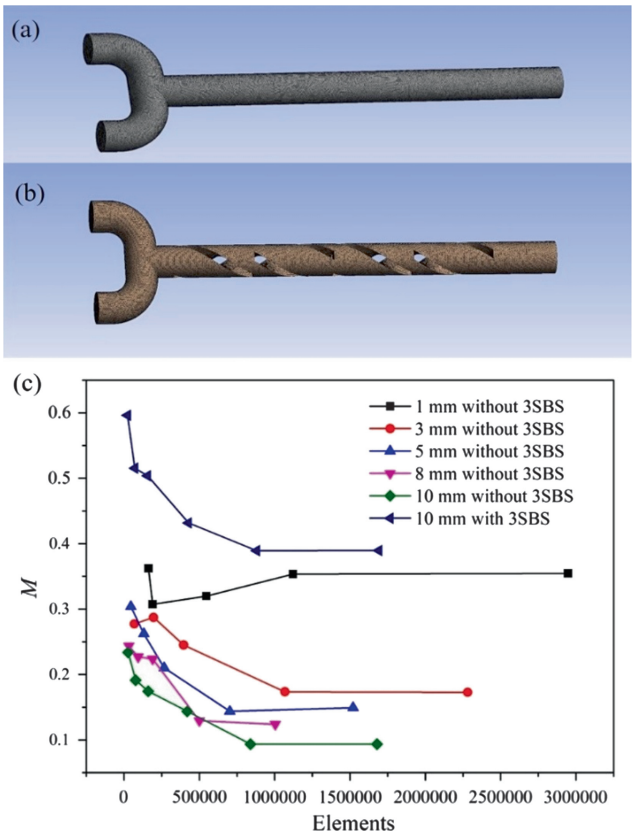

Fig. 2. (a) Mesh of 10 mm YSTM without 3SBS; (b) mesh of 10 mm YSTM with 3SBS; (c) effects of mesh elements on mixing efficiency.

equals 1, the reaction solutions are completely segregated. While X_s equals 0, the reaction solutions are completely mixed.

The value of $C_{I_3^-}$ can be calculated by:

$$C_{I_3^-}=\frac{A_\varepsilon}{K_\varepsilon} \tag{8}$$

where A_ε represents the absorbance of the solution under 353 nm-wavelength UV; K_ε is equal to 26047 L·mol^{-1} [41].

After obtaining $C_{I_3^-}$, the value of C_{I_2} can be calculated by:

$$\frac{5}{3}C_{I_2}^2+\left(\frac{8}{3}C_{I_3^-}-C_{I^-,0}\right)C_{I_2}+\frac{C_{I_3^-}}{K_B}=0 \tag{9}$$

where K_B is the equilibrium constant of reaction (c), and it equals 702 L·mol^{-1} under 25 °C [41].

In the experimental process, the chemical agents including H_2SO_4, KI, KIO_3, H_3BO_3 and NaOH were all at the analytical purity. The initial concentrations of the reaction solution at inlet-1 and inlet-2 are shown in Table 1 [41]. The reaction liquid flowing from inlet-1 was diluted by 98% H_2SO_4 solution. The reaction liquids from inlet-2 were premixed before flowing into the reactor. After the experiment, the absorbance of the solution was measured by UV–Vis spectrometer (G10S UV–Vis, Thermo Fisher Scientific, USA).

3. Results and Discussion

3.1. Scale effects of fluid flow in YSTM

In order to improve the capacity of the liquid–liquid homogeneous reactor, the effect of D_Y on the mixing performance of YSTM was studied. Reynolds number relates to the velocity, density and viscosity of the fluids, and it is considered to be a more comprehensive parameter to obtain a conclusive information for fluids mixing. However, in this study, the viscosity and density of the fluids are fixed. And if the Reynolds number remains constant, it means that the total flow velocity of the mixer with small pipe diameter is smaller. This is not conducive to the study of the scale effect of YSTM under high capacity. Therefore, the total flow velocity is fixed at 0.01 m·s^{-1} and flow velocity ratio is fixed at 1. The length is selected at 5, 30, 55, 80 and 105 mm, respectively. Through simulation, the mass fraction distribution of the fluid in YSTM is obtained. Fig. 4(a) and (b) show the mass fraction distribution of 1 mm and 10 mm YSTM with various lengths. It can be clearly seen that with the increase of the length, the mixing efficiency is enhanced gradually. The reason is that with the increase of the length, the fluids have more mixing time. For 1 mm, the fluid has been almost completely mixed at the length of 30 mm. While for 10 mm, the mixing effect is still bad when the length is 105 mm. Fig. 4(c) shows the effects of D_Y on mixing efficiency. With the increase of D_Y, the mixing efficiency reduces gradually. The reason is that with the increase of D_Y, the diffusion distance of fluid increases.

Fig. 4(d) shows the effects of t on mixing efficiency. With the increase of t, the mixing efficiency is enhanced gradually. Moreover, the less time it takes to achieve near complete mixing when the pipe diameter is smaller. For example, when D_Y is 1 mm, the mixing index at 1050 ms is 0.7038. While for 3 mm, it is 0.2904. With the increase of D_Y, the mass transfer distance between fluids increases, and it takes longer time and longer channel length to achieve efficient mixing. Additionally, the mixing efficiency of 10 mm YSTM at 105 mm is 0.1762, which means the mixing efficiency is reduced by 75.0%. Therefore, there is a scale effect that the mixing efficiency decreases with the increase of D_Y in YSTM.

3.2. Microfluidic field strategy and enhancement mechanism

3.2.1. Microfluidic field strategy

Due to the scale effect, there is a competition mechanism between mixing efficiency and treatment capacity in YSTM. When

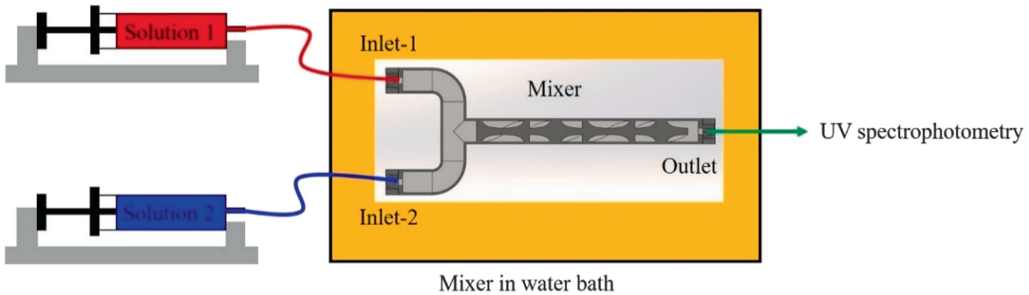

Fig. 3. Experimental setup of the verification experiments.

Table 1
The initial reaction solutions concentrations in the homogeneous case

Position	Solution	Concentration/mol·L^{-1}
Inlet-1	H_2SO_4	0.0350
Inlet-2	KI	0.0117
	KIO_3	0.0023
	H_3BO_3	0.0909
	NaOH	0.0909

D_Y is 1 mm, YSTM has the low treatment, despite it has high mixing efficiency. For 10 mm, it is opposite to that of 1 mm. Therefore, it is necessary to enhance the mixing efficiency of YSTM with D_Y of 10 mm to eliminate the scale effect. As shown in Fig. 5, microfluidic field strategy is adopted to enhance and enlarge the continuous flow chemical process, and 3SBS is embedded into the channel of 10 mm YSTM to form secondary flow disturbance. Under the enhancement of the secondary flow disturbance caused by 3SBS, the mixing efficiency in the channel of 10 mm YSTM is expected to be comparable to that in the microscale channel. Finally, the mixing efficiency and treatment capacity of the chemical process will be both at a high level.

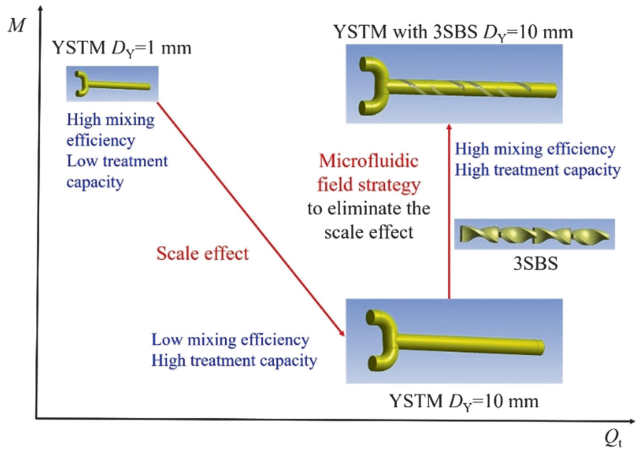

Fig. 5. Schematic diagram of microfluidic field strategy.

3.2.2. Enhancement mechanism of 3SBS

In this work, 3SBS is designed to induce the secondary flow of the Goertler vortex [38] with continuously changing direction, which has great potential to promote fluid mixing. In order to confirm the enhancement effect of 3SBS on mixing efficiency, velocity streamlines of 10 mm YSTM without and with 3SBS are obtained, as shown in Fig. 6. For 10 mm YSTM without 3SBS, the main vortex is formed on the boundary of two fluids, but with the increase of flow distance, the intensity of vortex gradually decreases, which will lead to the bad mixing efficiency. For 10 mm YSTM with 3SBS, the fluids moves along the spiral baffles, due to the centrifugal force, which causes the streamline to bend along the helical baffle. Compared with 10 mm YSTM without 3SBS, the velocity streamline of 10 mm YSTM with 3SBS has more secondary flow vortices produced on the radial equidistant section at the second

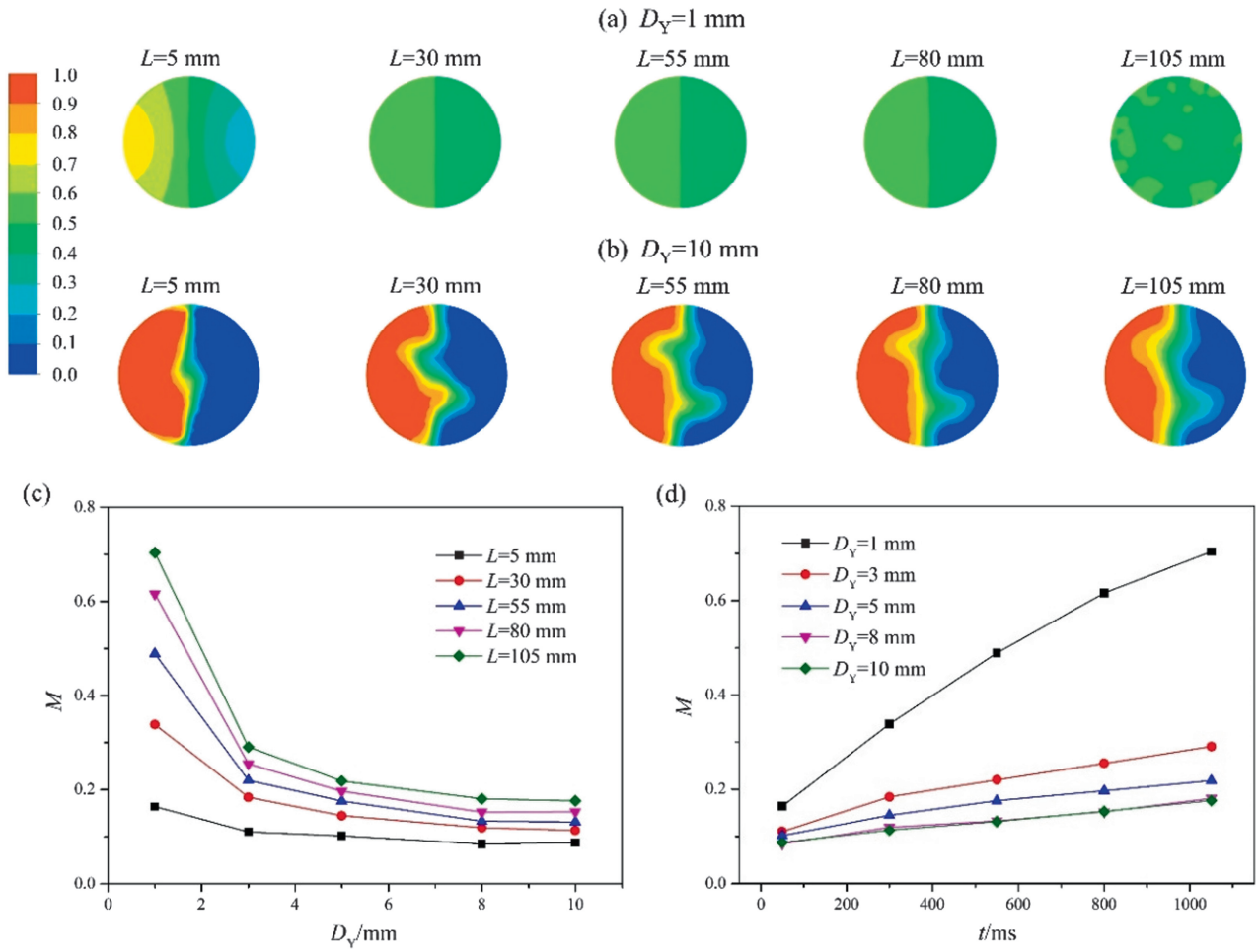

Fig. 4. Mass fraction distributions of the fluid in radial section of (a) 1 mm YSTM and (b) 10 mm YSTM. Effects of (c) D_Y and (d) t on mixing efficiency.

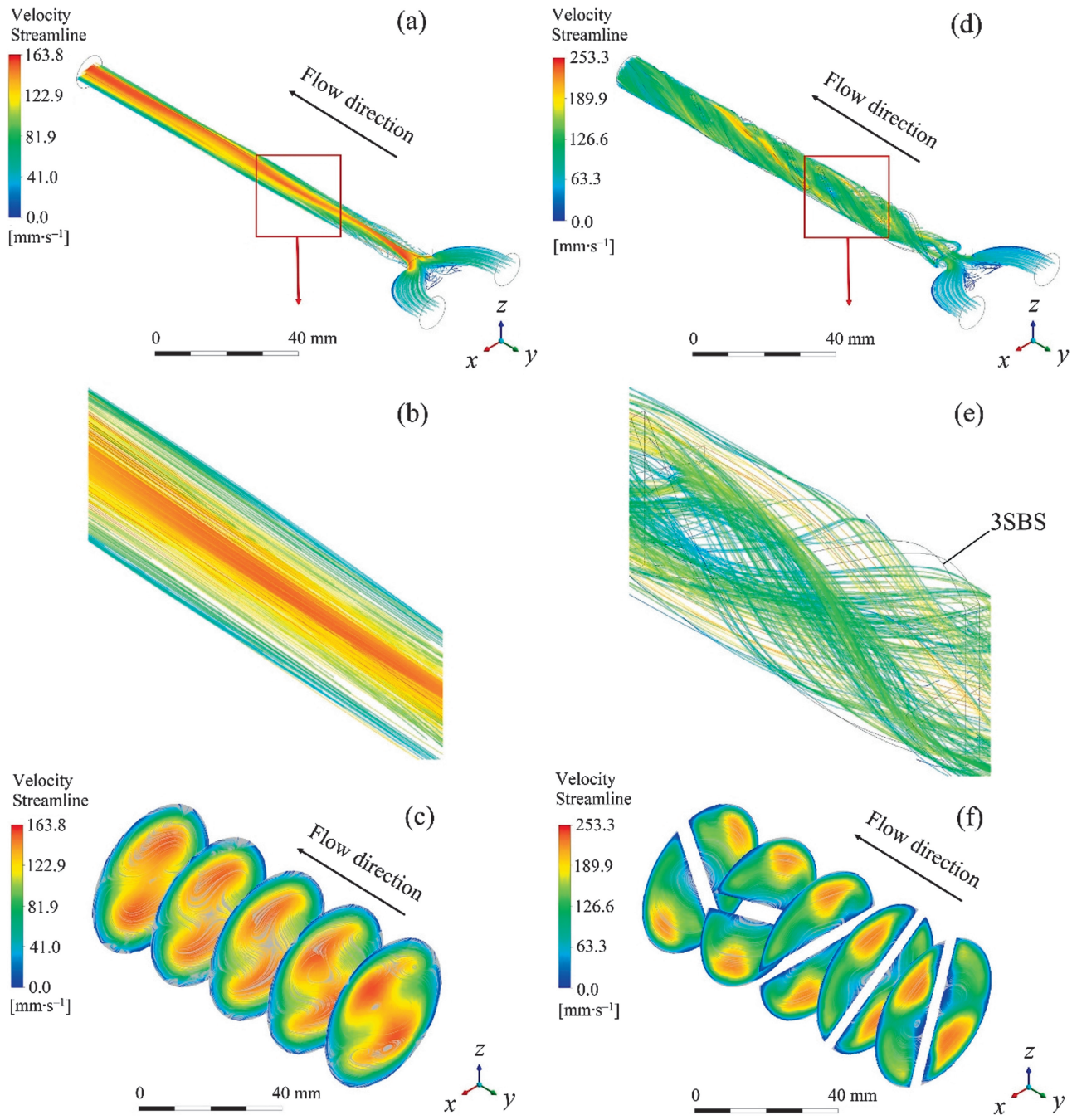

Fig. 6. Velocity streamline of global area, selected area and equidistant radial sections of (a)–(c) 1 mm YSTM and (d)–(f) 10 mm YSTM without 3SBS.

spiral baffle position, which is likely to promote the fluid mixing. The fluids moves along the spiral baffles, and the streamline bends along the helical baffle due to the centrifugal force. Furthermore, the secondary flow vortexes with opposite rotation direction are produced, and the position of secondary flow vortices are changing constantly. It confirms that confinement of trajectories along the spiral baffles induces counter rotating transversal flows. Therefore, 3SBS is considered to be a suitable structure for enhancing the mixing efficiency in YSTM.

3.3. Enhancement effects of 3D spiral baffle structure

In order to verify the enhancement effect of liquid–liquid homogeneous, the mixing efficiencies in 10 mm YSTM with and without the optimal 3SBS are compared. The total length of the mixing zone is fixed at 130 mm. The total flow velocity is fixed at 0.01 $m \cdot s^{-1}$ and flow velocity ratio is fixed at 1. The mass fraction of liquid-2 on the radial section with axial length of 5, 30, 55, 80, 105 and 130 mm was selected as the research object. Through simulation, the mass fraction distribution of the fluids in YSTM without 3SBS is obtained as shown in Fig. 7.

Compared with 10 mm YSTM without 3SBS, the mixing efficiency of the fluids in the 10 mm YSTM with 3SBS is improved obviously at different radial sections. The improvement of mixing efficiency of 10 mm YSTM is caused by the 3SBS with the structural parameters of baffle thickness (a), torsion angle (θ_1), length of spiral baffle (L_s) and angle between baffles (θ_2). After adding baffle, the equivalent diameter of YSTM is reduced. The increase of baffle thickness leads to the decrease of equivalent diameter in the mixer and the increase of extrusion strength of fluid pipe wall and baffle. The

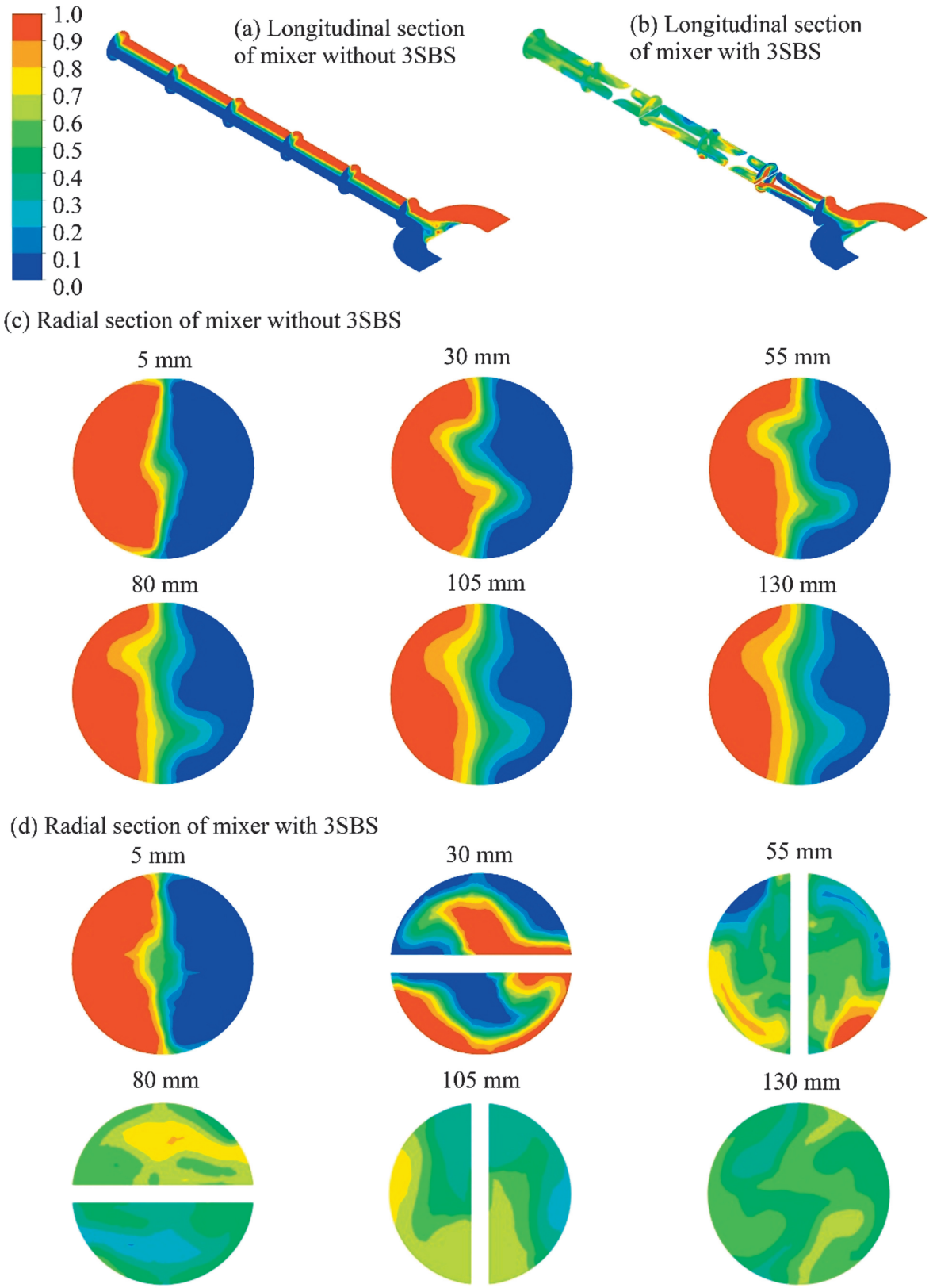

Fig. 7. Mass fraction of liquid-2 on longitudinal section of 10 mm YSTM without 3SBS (a) and with 3SBS (b); radial sections of 10 mm YSTM without 3SBS (c) and with 3SBS (d).

torsion angle makes the direction of secondary flow disturbance continuously changed. The torsion of the baffle unit effectively enhances the convective mass transfer of the fluid. The length of spiral baffle and the angle between baffles determine the frequency and direction of convective mass transfer. Therefore, the 3SBS can enhance the mixing efficiency of liquid–liquid homogeneous fluid.

3.4. Structure optimization of 3SBS

The structure of 3SBS is determined by baffle thickness, torsion angle, length of spiral baffle and angle between baffles, which are likely to affect the liquid–liquid homogeneous chemical process. In order to enhance the functional characteristics, the structure of 10 mm YSTM with 3SBS is optimized with mixing efficiency as the evaluation index.

3.4.1. Effects of baffle thickness on mixing efficiency

Firstly, the influence of baffle thickness on mixing efficiency is studied. The total flow velocity is fixed at 0.01 $m \cdot s^{-1}$ and flow velocity ratio is fixed at 1. The torsion angle is fixed at 180°. The baffle unit length is fixed at 25 mm. The baffle thickness is adjusted to 1, 2, 3, 4 and 5 mm, respectively. The results of mixing efficiency in 10 mm YSTM with 3SBS at different baffle thickness are shown in Fig. 8. It can be clearly seen that the mixing efficiency is enhanced gradually with the increase of baffle thickness. When baffle thickness is 1 mm, four baffle units fail to bring the fluid to a basically complete mixing state. When baffle thickness is 2 mm or 3 mm, four baffle units are needed to achieve basically complete mixing state, which takes about 1050 ms. While for 4 mm and 5 mm, three baffle units and approximately 800 ms are needed. Compared with 4 mm, the mixing efficiency of YSTM with baffle thickness of 5 mm has higher mixing efficiency. Therefore, the optimal thickness of the baffle is considered to be 5 mm.

3.4.2. Effects of torsion angle on mixing efficiency

The second factor affecting the mixing efficiency is the torsion angle. The total flow velocity is fixed at 0.01 $m \cdot s^{-1}$ and flow velocity ratio is fixed at 1. The baffle thickness is fixed at 1 mm. The baffle unit length is fixed at 25 mm. The angle between adjacent baffles is fixed at 90°. The torsion angle is adjusted to 180°, 360°, 540° and 720°, respectively. The results of mixing efficiency in 10 mm YSTM with 3SBS at different torsion angle are shown in Fig. 9. It can be clearly seen that the mixing efficiency first increases and then decreases with the increase of torsion angle. For 180°, four baffle units fail to achieve basically complete mixing. For 360°, it has reached the state of basically complete mixing at the third baffle, and the time needed is about 800 ms. For 540° and 720°, four baffle units and approximately 1000 ms are needed. The mixing efficiency reaches the highest when the torsion angle is 360°. When the adjacent baffle angle is fixed at 90°, the mixing process of fluids can be divided into two parts, namely, the mixing of fluids in one baffle unit and the mixing between adjacent baffle units. Increasing the torsion angle is beneficial to strengthen the mixing process in the baffle unit. Additionally, with the increase of torsion angle, the curvature of fluid flow along the baffle increases and more secondary flow vortices are produced, which

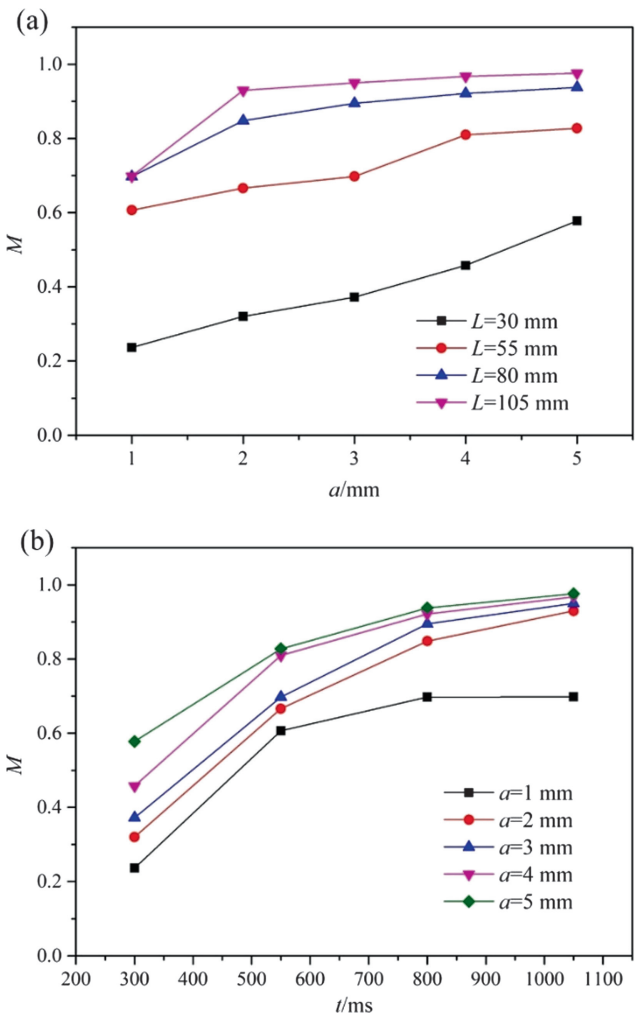

Fig. 8. Effects of (a) baffle thickness and (b) mixing time on mixing efficiency with variation of baffle thickness.

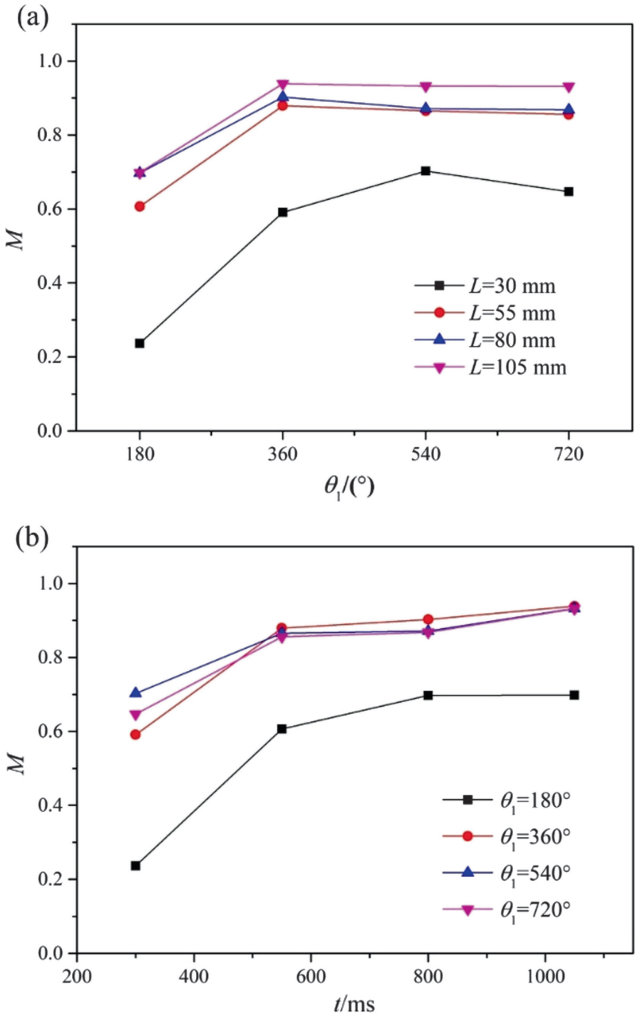

Fig. 9. Effects of (a) torsion angle and (b) mixing time on mixing efficiency with variation of torsion angle.

is beneficial to promote the mixing of fluid. However, it also leads to the longer residence time of the fluid in the baffle unit, reduces the frequency of strengthening the mixing process between adjacent baffles, and weakens the mixing of the fluid between adjacent baffle units. This means that the mixing index first increases and then decreases with the increase of torsion angle. Therefore, the optimal torsion angle is selected as 360°.

3.4.3. Effects of the length of spiral baffle on mixing efficiency

The third factor affecting the mixing efficiency is the length of spiral baffle. The total flow velocity is fixed at 0.01 $m \cdot s^{-1}$ and flow velocity ratio is fixed at 1. The baffle thickness is fixed at 3 mm. The torsion angle is fixed at 180°. The length of spiral baffle is adjusted to 5, 10, 20, 25 and 50 mm, respectively. The results of mixing efficiency in 10 mm YSTM with 3SBS at different baffle unit lengths are shown in Fig. 10. It can be clearly seen that the mixing efficiency is reduced gradually with the increase of the length of spiral baffle. When L_s is 50 mm, there are only two spiral baffle units in the mixing area of 100 mm. Although the two helical baffles are vertically staggered, the fluid failed to reach the state of complete mixing. When L_s is reduced to 25, 20, 10 and 5 mm, the number of spiral baffles in 100 mm mixing area is 4, 5, 10 and 20 respectively. When L_s is 5, 10, 20, 25 and 50 mm, the frequency of the vertical cross direction is 20, 40, 50, 100 and 200, respectively. At the same time or mixing length, increasing the number of vertical cross direction is beneficial to promote the mixing of fluid. Therefore, the optimal length of spiral baffle is 5 mm in this work.

3.4.4. Effects of the angle between baffles on mixing efficiency

The last factor that affects the mixing efficiency is the angle between baffles. The total flow velocity is fixed at 0.01 $m \cdot s^{-1}$, the flow velocity ratio is fixed at 1, the baffle thickness is fixed at 5 mm, and the baffle unit length is fixed at 25 mm. The results of mixing efficiency in 10 mm YSTM with 3SBS with different angle between baffles are shown in Fig. 11. The baffle angles are adjusted to 0°, 45°, 90° and 135°, respectively. It can be clearly seen that the mixing efficiency increases and then decreases as the angle between the baffles increases. The mixing efficiency reaches the highest when the angle is 90°. For a baffle angle of 90°, the mixing is almost complete at the second baffle and it takes about 550 ms. For 45° and 135°, three baffle units and about 800 ms are needed. For 0°, more baffle units and more time are required. As the angle between the baffles increases, the secondary flow vortex generated by the fluid flowing through the baffles also increases, but the secondary flow vortex generated gradually decreases when the angle is greater than 90°. Therefore, the optimal angle between the baffles is 90°.

After the above geometry optimization based on the mixing efficiency, the baffle thickness, torsion angle, length of spiral baffle and angle between baffles are determined as 5 mm, 360°, 5 mm

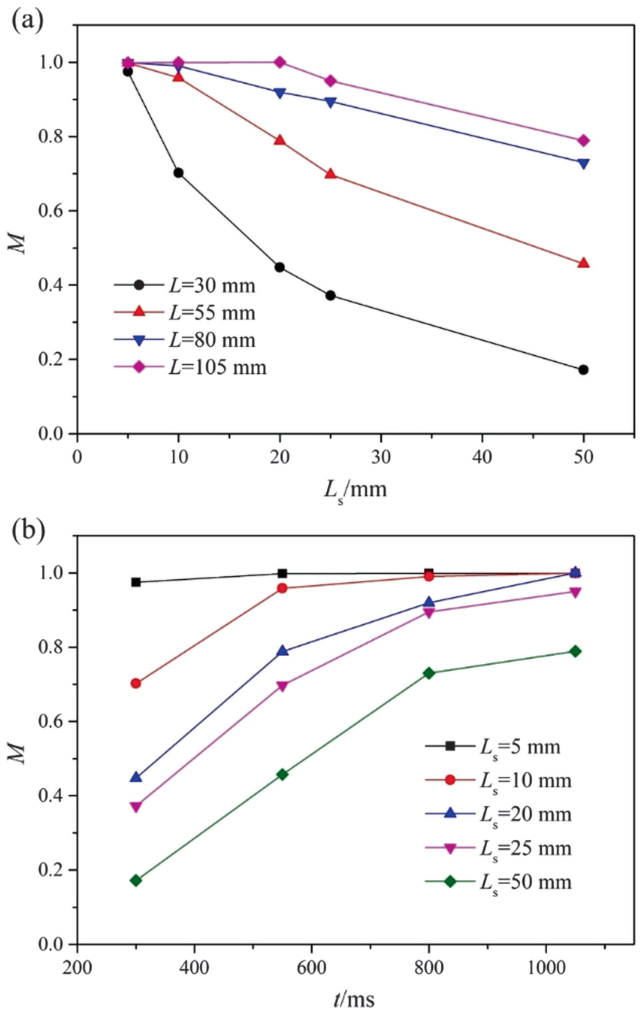

Fig. 10. (a) Effects of the length of spiral baffle on mixing efficiency and (b) effects of mixing time on mixing efficiency with variation of the length of spiral baffle.

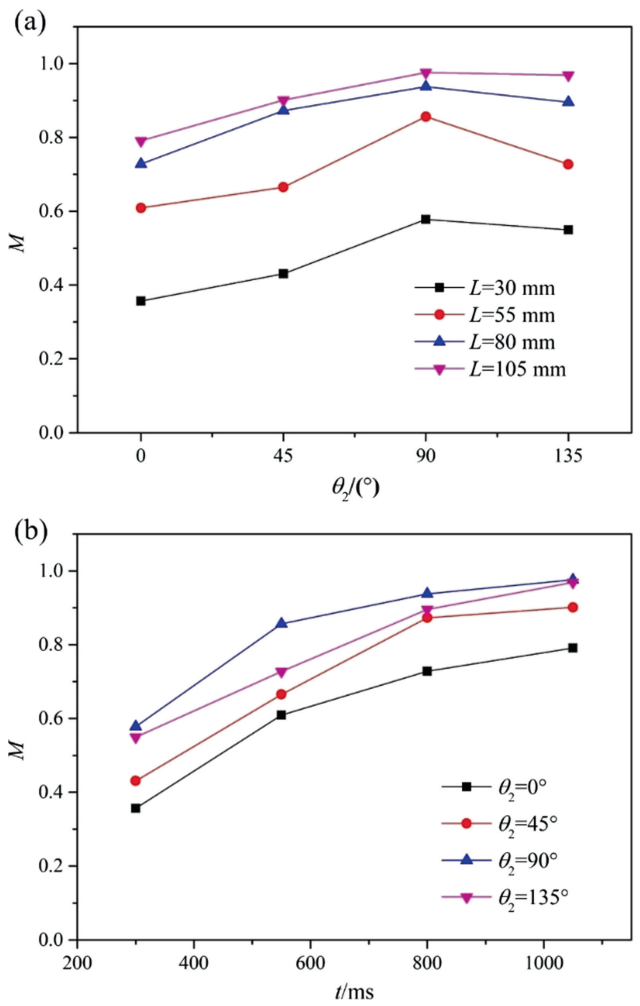

Fig. 11. Effects of (a) angle between baffles and (b) mixing time on mixing efficiency with variation of angle between baffles.

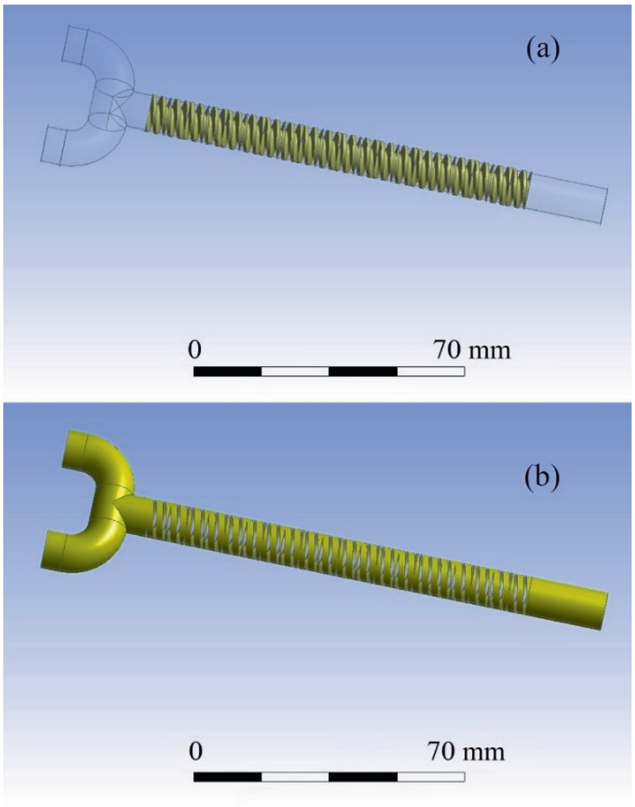

Fig. 12. (a) The optimal geometry and (b) the internal fluid region of 10 mm YSTM with 3SBS.

and 90°, respectively. The optimal geometry and the internal fluid region of 10 mm YSTM with 3SBS are shown in Fig. 12.

3.5. Experimental verification

In order to verify the effect of microfluidic field strategy and the results of simulation experiments, homogeneous verification experiments were conducted. The Villermaux–Dushman parallel competing reaction was used to evaluate the homogeneous case. The flow velocity in the verification test is fixed at 0.01 $m \cdot s^{-1}$. For the simulation, when the length of the mixer is long enough, the fluid can be completely mixed at the outlet. In this case, it is difficult to distinguish the mixing effect of different mixers simply by the value of mixing efficiency. However, the time required for different mixers to achieve basically complete mixing is different. Therefore, $t_{0.9}$ can effectively quantify the mixing effect of the mixers in the simulation. For homogeneous experiments, X_s means the segregation index of the reaction. If the mixing efficiency is high, the reaction with fast chemical reaction rate is more likely to occur. Therefore, for the simulation results, the mixing efficiency of the mixer was characterized by $t_{0.9}$. While for the experimental results, it was characterized by X_s. Fig. 13 shows the $t_{0.9}$ and X_s of YSTM with different mixer structures.

For the simulation results, the shorter $t_{0.9}$ means the higher mixing efficiency. It indicates that $t_{0.9}$ increases from 14360 ms to 90680 ms when D_Y increases from 1 mm to 10 mm. Compared with YSTM without 3SBS, it is can be clearly seen that the time required for the fluid to reach complete mixing are significantly reduced after inserting the 3SBS in 10 mm YSTM. For the initial 10 mm YSTM with 3SBS, the mixing efficiency can be comparable to that in the 1 mm YSTM without 3SBS, and $t_{0.9}$ is reduced to 9290 ms, which is shorter than 1 mm YSTM without 3SBS. After

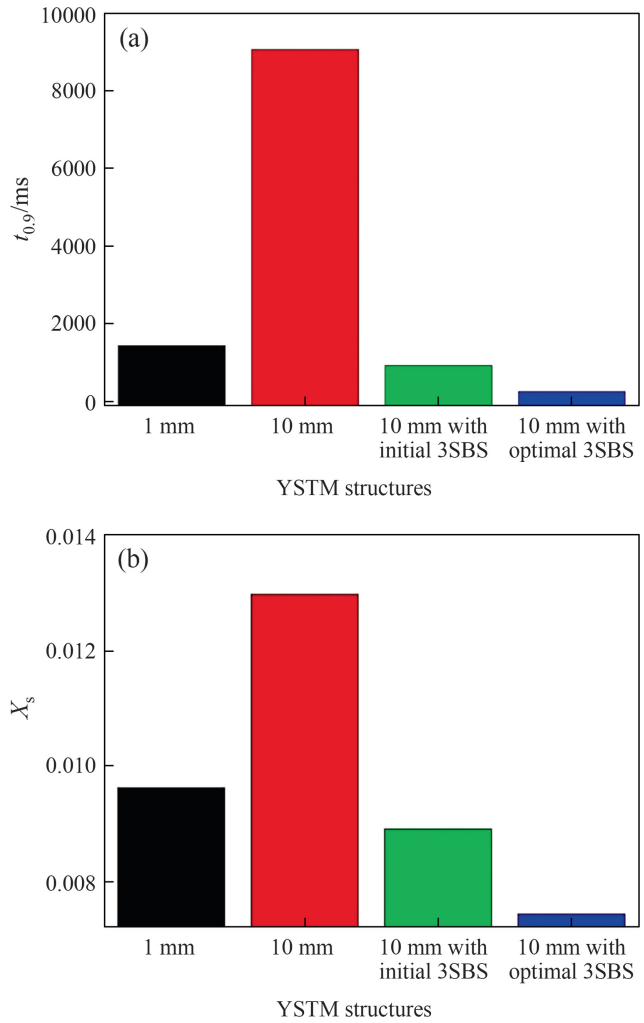

Fig. 13. Comparison between YSTM structures on the $t_{0.9}$ obtained by simulation (a) and X_s obtained by experiment (b).

optimizing the structure of 3SBS, $t_{0.9}$ is significantly reduced to 2580 ms, which is 18% of that of 1 mm YSTM. For the experimental results, the smaller X_s means the higher mixing efficiency. By the comparison between 1 mm YSTM, 10 mm YSTM, 10 mm YSTM with 3SBS before and after optimization, it can be clearly seen that $t_{0.9}$ and X_s have the same trend. Therefore, the homogeneous simulation can be proved by the experimental results, and the microfluidic field strategy achieves scale-up on the premise of ensuring high mixing efficiency.

4. Conclusions

There is a scale effect in YSTM that the mixing efficiency in homogeneous chemical process decrease with the increase of D_Y. Compared with 1 mm YSTM, the diffusion distance of the fluid becomes longer with the increase of the diameter of YSTM, which leads to the lower mixing efficiency in 10 mm YSTM. Microfluidic field strategy is adopted to enhance and enlarge the continuous flow chemical process, and 3SBS is embedded into the channel of YSTM, which leads to the formation of secondary flow disturbance with continuous change of direction. Velocity streamline confirms that confinement of trajectories along the spiral baffles induces counter rotating transversal flows, and 3SBS is considered to be a suitable structure for enhancing the mixing efficiency in YSTM. Under the secondary flow disturbance caused by the 3SBS, the mix-

ing efficiency in homogeneous chemical process can be obviously enhanced. The 10 mm YSTM with 3SBS are optimized and the optimal baffle thickness, torsion angle, length of spiral baffle and angle between baffles are determined as 5 mm, 360°, 5 mm and 90°, respectively. Compared to the 1 mm YSTM without 3SBS, 10 mm YSTM with 3SBS increased the treatment capacity by 100 times, shortened the basic complete mixing time by 0.85 times, which proves the potential of microfluidic field strategy in chemical processes scale-up. The main shortcoming of the current work is the applicable flow velocity range. In this study, the total velocity of the 10 mm mixer with 3SBS is not more than 0.01 $m \cdot s^{-1}$. The reason is that it is difficult to realize the verification experiment at higher flow rate in the laboratory. Additionally, the size of the YSTM mixer is only enlarged to 10 mm. Therefore, in the future, we will continue to increase the total flow velocity and expand the size of the mixer to further improve the processing capacity. All the findings reported provide useful references for enhancement and scale up of liquid–liquid homogeneous by the way of microfluidic field strategy.

Declaration of Competing Interest

The authors declare that they have no known competing financial interests or personal relationships that could have appeared to influence the work reported in this paper.

Acknowledgements

The research has been supported by the National Key Research and Development Program of China (2021YFC2101900 and 2019YFA0905000); National Natural Science Foundation of China (21908094, 21776130 and 22078150); Nanjing International Joint Research and Development Project (202002037); Top-notch Academic Programs Project of Jiangsu Higher Education Institutions.

References

[1] J.B. Zimmerman, P.T. Anastas, H.C. Erythropel, W. Leitner, Designing for a green chemistry future, *Science* 367 (6476) (2020) 397–400.
[2] N. Zhu, X. Hu, Z. Fang, K. Guo, Chemoselective polymerizations, *Prog. Polym. Sci.* 117 (2021) 101397.
[3] J.Y. Liao, S.L. Zhang, Z.S. Wang, X. Song, D.L. Zhang, R. Kumar, J. Jin, P. Ren, H.Z. You, F.E. Chen, Transition-metal catalyzed asymmetric reactions under continuous flow from 2015 to early 2020, *Green Synth. Catal.* 1 (2) (2020) 121–133.
[4] Y. Liu, X.Y. Jiang, Why microfluidics? Merits and trends in chemical synthesis, *Lab Chip* 17 (23) (2017) 3960–3978.
[5] D. Wang, T. Zhang, Y.C. Yang, S.W. Tang, Simulation and design microreactor configured with micromixers to intensify the isobutane/1-butene alkylation process, *J. Taiwan Inst. Chem. Eng.* 98 (2019) 53–62.
[6] W.Z. Guo, H.J. Heeres, J. Yue, Continuous synthesis of 5-hydroxymethylfurfural from glucose using a combination of $AlCl_3$ and HCl as catalyst in a biphasic slug flow capillary microreactor, *Chem. Eng. J.* 381 (2020) 122754.
[7] L.L. Lin, H. Quoc Pho, L. Zong, S.R. Li, N. Pourali, E. Rebrov, N. Nghiep Tran, K. Ostrikov, V. Hessel, Microfluidic plasmas: Novel technique for chemistry and chemical engineering, *Chem. Eng. J.* 417 (2021) 129355.
[8] S.F. Zhao, J.W. Wu, P. Zhu, H.M. Xia, C. Chen, R.Q. Shen, Microfluidic platform for preparation and screening of narrow size-distributed nanoscale explosives and supermixed composite explosives, *Ind. Eng. Chem. Res.* 57 (39) (2018) 13191–13204.
[9] S.F. Zhao, C. Chen, P. Zhu, H.M. Xia, J.Y. Shi, F. Yan, R.Q. Shen, Passive micromixer platform for size- and shape-controllable preparation of ultrafine HNS, *Ind. Eng. Chem. Res.* 58 (36) (2019) 16709–16718.
[10] N.R. Visaveliya, J.M. Köhler, Hierarchical assemblies of polymer particles through tailored interfaces and controllable interfacial interactions, *Adv. Funct. Mater.* 31 (9) (2021) 2007407.
[11] K.K. Kang, B. Lee, C.S. Lee, Recent progress in the synthesis of inorganic particulate materials using microfluidics, *J. Taiwan Inst. Chem. Eng.* 98 (2019) 2–19.
[12] S. Ebadi, K. Ghasemipanah, E. Alaie, A. Rashidi, A. Khataee, COD removal from gasfield produced water using photoelectrocatalysis process on coil type microreactor, *J. Ind. Eng. Chem.* 98 (2021) 262–269.
[13] N. Wang, Q. Wang, Y.Q. Geng, X. Sun, D.K. Wu, Y.Z. Yang, Recovery of Au(III) from acidic chloride media by homogenous liquid–liquid extraction with UCST-type ionic liquids, *ACS Sustain. Chem. Eng.* 7 (24) (2019) 19975–19983.
[14] H.H. Shi, K.X. Nie, B. Dong, M.Q. Long, H. Xu, Z.C. Liu, Recent progress of microfluidic reactors for biomedical applications, *Chem. Eng. J.* 361 (2019) 635–650.
[15] M. Ugrinic, A. deMello, T.Y.D. Tang, Microfluidic tools for bottom-up synthetic cellularity, *Chem* 5 (7) (2019) 1727–1742.
[16] Y.C. Zhao, G.W. Chen, Progress in research on numbering-up of microchemical system, *Sci. Sin.-Chim.* 45 (1) (2015) 16–23.
[17] J.S. Zhang, K. Wang, A.R. Teixeira, K.F. Jensen, G.S. Luo, Design and scaling up of microchemical systems: A review, *Annu. Rev. Chem. Biomol. Eng.* 8 (2017) 285–305.
[18] M. Oelgemoeller, Highlights of photochemical reactions in microflow reactors, *Chem. Eng. Technol.* 35 (7) (2012) 1144–1152.
[19] A. Yavorskyy, O. Shvydkiv, N. Hoffmann, K. Nolan, M. Oelgemöller, Parallel microflow photochemistry: Process optimization, scale-up, and library synthesis, *Org. Lett.* 14 (17) (2012) 4342–4345.
[20] M. Qiu, L. Zha, Y. Song, L. Xiang, Y.H. Su, Numbering-up of capillary microreactors for homogeneous processes and its application in free radical polymerization, *React. Chem. Eng.* 4 (2) (2019) 351–361.
[21] G.N. Ahn, T. Yu, H.J. Lee, K.W. Gyak, J.H. Kang, D. You, D.P. Kim, A numbering-up metal microreactor for the high-throughput production of a commercial drug by copper catalysis, *Lab Chip* 19 (20) (2019) 3535–3542.
[22] C.X. Cao, D. Dang, Y.K. Li, J. Xu, Y. Cheng, Strategy for multiscale numbering-up of microstructured catalytic reactors: A numerical study based on the resistance network model, *J. Taiwan Inst. Chem. Eng.* 98 (2019) 70–77.
[23] H. Han, J.H. Yoon, G.R. Yi, W.I. Choi, J.M. Lim, High-speed continuous production of polymeric nanoparticles with improved stability using a self-aligned coaxial turbulent jet mixer, *J. Ind. Eng. Chem.* 97 (2021) 411–416.
[24] J.M. Lim, A. Swami, L.M. Gilson, S. Chopra, S. Choi, J. Wu, R. Langer, R. Karnik, O. C. Farokhzad, Ultra-high throughput synthesis of nanoparticles with homogeneous size distribution using a coaxial turbulent jet mixer, *ACS Nano* 8 (6) (2014) 6056–6065.
[25] Y. Xie, Q. Chen, G.M. Huang, Y.J. Wang, W.G. Hu, Z.R. Yan, X. Wang, J. Huang, M. T. Gao, W.Y. Fei, G.S. Luo, Scaling up microreactors for kilogram-scale synthesis of piperacillin: Experiments and computational fluid dynamics simulations, *AIChE J.* 67 (7) (2021) e17231.
[26] D. Cheng, X. Feng, C. Yang, Z.S. Mao, Modelling and experimental investigation of micromixing of single-feed semi-batch precipitation in a liquid–liquid stirred reactor, *Chem. Eng. J.* 293 (2016) 291–301.
[27] W. Raza, S. Hossain, K.Y. Kim, A review of passive micromixers with a comparative analysis, *Micromachines* 11 (5) (2020) E455.
[28] M. Bayareh, M.N. Ashani, A. Usefian, Active and passive micromixers: A comprehensive review, *Chem. Eng. Process. Process. Intensif.* 147 (2020) 107771.
[29] H.E. Yang, G.C. Yao, D.S. Wen, Efficient mixing enhancement by orthogonal injection of shear-thinning fluids in a micro serpentine channel at low Reynolds numbers, *Chem. Eng. Sci.* 235 (2021) 116368.
[30] C.S. Shin, P.L. Baldeck, Y.M. Nie, Y.H. Lee, Z.D. Lin, C.C. Chiang, C.L. Lin, Design and evaluation of a 3D multi-manifold micromixer realized by a double-Archimedes-screw for rapid mixing within a short distance, *J. Taiwan Inst. Chem. Eng.* 120 (2021) 59–66.
[31] C.Y. Lee, W.T. Wang, C.C. Liu, L.M. Fu, Passive mixers in microfluidic systems: A review, *Chem. Eng. J.* 288 (2016) 146–160.
[32] H.L. Lv, X.Y. Chen, X.W. Zeng, Optimization of micromixer with Cantor fractal baffle based on simulated annealing algorithm, *Chaos Soliton. Fract.* 148 (2021) 111048.
[33] H.L. Lv, X.Y. Chen, New insights into the mechanism of fluid mixing in the micromixer based on alternating current electric heating with film heaters, *Int. J. Heat Mass Transf.* 181 (2021) 121902.
[34] H.L. Lv, X.Y. Chen, X.Y. Wang, X.W. Zeng, Y.B. Ma, A novel study on a micromixer with Cantor fractal obstacle through grey relational analysis, *Int. J. Heat Mass Transf.* 183 (2022) 122159.
[35] M.Z. Guo, X.J. Hu, F. Yang, S. Jiao, Y.J. Wang, H.Y. Zhao, G.S. Luo, H.M. Yu, Mixing performance and application of a three-dimensional serpentine microchannel reactor with a periodic vortex-inducing structure, *Ind. Eng. Chem. Res.* 58 (29) (2019) 13357–13365.
[36] X. Chao, F.S. Xu, C.Q. Yao, T.T. Liu, G.W. Chen, CFD simulation of internal flow and mixing within droplets in a T-junction microchannel, *Ind. Eng. Chem. Res.* 60 (16) (2021) 6038–6047.
[37] Y.Y. Liu, Q.K. Zhao, J. Yue, C.Q. Yao, G.W. Chen, Effect of mixing on mass transfer characterization in continuous slugs and dispersed droplets in biphasic slug flow microreactors, *Chem. Eng. J.* 406 (2021) 126885.
[38] W.H. Chen, R. Jan, The torsion effect on fully developed laminar flow in helical square ducts, *J. Fluids Eng.* 115 (2) (1993) 292–301.
[39] X.Y. Chen, T.C. Li, H. Zeng, Z.L. Hu, B.D. Fu, Numerical and experimental investigation on micromixers with serpentine microchannels, *Int. J. Heat Mass Transf.* 98 (2016) 131–140.
[40] J.W. Wu, H.M. Xia, Y.Y. Zhang, S.F. Zhao, P. Zhu, Z.P. Wang, An efficient micromixer combining oscillatory flow and divergent circular chambers, *Microsyst. Technol.* 25 (7) (2019) 2741–2750.
[41] D. Wang, G.Z. Ye, J.M. Mai, X.M. Chen, Y.Q. Yang, Y. Li, X.J. Chen, J. Chen, Novel micromixer with complex 3D-shape inner units: Design, simulation and additive manufacturing, *Comput. Modeling Eng. Sci.* 123 (3) (2020) 1061–1077.
[42] M. Jasińska, Test reactions to study efficiency of mixing, *Chem. Process. Eng.* 36 (2) (2015) 171–208.